Theoretical Analysis of the Structural and Electronic Properties of Metalloporphyrin π-Cation Radicals

Hajime Hirao,[†] Sason Shaik,*[,†] and Pawel M. Kozlowski*[,†,‡,§]

Department of Organic Chemistry and the Lise Meitner-Minerva Center for Computational Quantum Chemistry, The Hebrew University of Jerusalem, 91904 Jerusalem, Israel, and Department of Chemistry, University of Louisville, Louisville, Kentucky 40292

Received: October 11, 2005; In Final Form: February 10, 2006

A method for analyzing the A_{1u}/A_{2u} contents of metalloporphyrin π-cation radicals is developed and applied to a series of unsubstituted planar metalloporphines (MPs) (M = Cr, Mn, Fe, Co, Ni, Cu, and Zn). The structures and electronic properties of the MPs and their cation radicals were calculated by density functional theory (DFT) and subsequently analyzed. It was found that the MPs with small core sizes have a tendency to form A_{1u}-type radicals, while the MPs with large core size have a preference for an A_{2u}-type. Neither of these pure-state species, however, is stable under the D_{4h} symmetry, and both radical cation types are subject to pseudo-Jahn−Teller (pJT) distortion. The pJT distortion leads to structures with lower symmetry and states that have mixed character with respect to the A_{1u} and A_{2u} components. The degree of mixing could be estimated by employing orbital projection technique or a complementary spin density decomposition. Both techniques produce very similar results, pointing out that the frontier orbital, which becomes empty upon electron removal, plays a critical role in determining electronic properties.

Introduction

Metalloporphyrins (MPs, Figure 1) play an important role in biological systems where they serve as active species with the ability to bind ligands, facilitate light-harvesting photosynthetic reactions, transfer electrons, and catalyze enzymatic reactions.[1,2] There are many reasons why nature uses MPs in such a diverse way; however, redox chemistry appears to be one of the most important features among them. Oxidation of MPs may occur at the central metal, at the porphyrin ligand, or at both locations. The latter, doubly oxidized MP structures have been implicated in the catalytic cycles of heme peroxidases,[3] P450 monooxygenases,[4] or catalases.[5] Characterization of MP π-cation radicals is thus of interest because of their widespread occurrences in nature and because of the unusual chemistry in which they participate.

Porphyrins have two closely spaced, nearly degenerate highest occupied molecular orbitals (HOMOs) of a_{1u} and a_{2u} symmetry in the D_{4h} molecular framework (Figure 2). The relative energies of these orbitals are influenced by several factors, such as the position and type of substituents on the porphyrin macrocycle, or the nature of the axial ligand(s) to the transition metal. As such, removal of an electron can lead to a radical with an A_{1u} or A_{2u} ground state, depending on which orbital lies higher in energy. An important question related to the intermediates of many oxidative heme enzymes and nonenzymatic MP radicals is whether they can be described as A_{1u}- or A_{2u}-type radicals. A great variety of experimental techniques, including UV−visible (UV−vis), electron paramagnetic resonance (EPR), NMR, magnetic circular dichroism (MCD), and vibrational spectroscopy, have been applied to address this issue and to analyze the molecular properties of π-cation radicals of MP.[6−17]

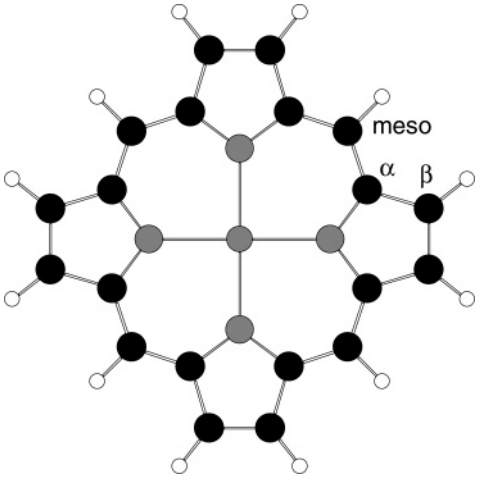

Figure 1. Molecular structure of metalloporphine (MP), with carbon atoms C_α, C_β, and C_{meso} labeled explicitly.

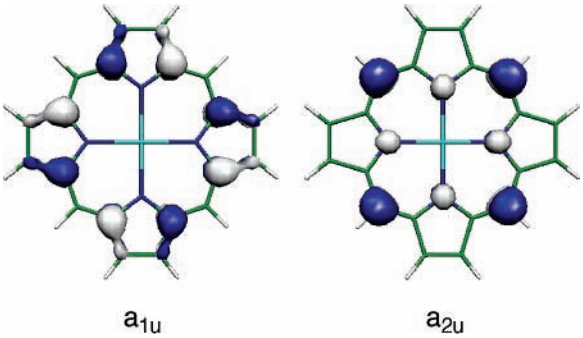

Figure 2. Plots (obtained with MOLEKEL software[27]) of two HOMOs of symmetry a_{1u} and a_{2u}.

* Corresponding authors. E-mail: sason@yfaat.ch.huji.ac.il (S.S.); pawel@louisville.edu (P.M.K.).
† The Hebrew University of Jerusalem.
‡ University of Louisville.
§ Fulbright Visiting Professor under the United States−Israeli Educational Foundation (USIEF).

10.1021/jp0558066 CCC: $33.50
Published on Web 04/19/2006

Among these techniques, resonance Raman (RR) spectroscopy[18,19] provides a powerful tool for probing the molecular and electronic structure of MPs. The frequencies of the RR bands are sensitive to changes in bonding and conformation, while their intensities are sensitive to the nature of the resonant electronic state. Although A_{1u} and A_{2u} may be reasonable approximate designations for the radical type, experimental data, including density profiles based on EPR spectroscopy[20] or the appearance of A_{2g} RR active modes at much lower frequencies,[19] strongly suggest that these states are frequently mixed. This is because the ground and excited states are subject to deformations (vibronic coupling), which lead to mixed-symmetry states. Indeed, the near-degeneracy of the frontier orbitals can be expected to produce a pseudo-Jahn−Teller (pJT) effect. The pJT effect exerts the most pronounced consequences on the porphyrin ring, leading to alternation of the bond lengths in the perimeter of the inner 16-membered ring. The bond alternation was observed in the X-ray structure of $[Zn(OEP^{\bullet})]^{+}$.[21,22]

Despite the importance of these radical cations and the large body of experimental data associated with them, relatively little attention has been given to elucidating their structural and electronic properties using methods of electronic structure calculations. Only several theoretical studies have been published that specifically addressed this issue.[23−25] For a long time, the pioneering work of Prendergast and Spiro[23] has been the only source of significant theoretical analysis of pJT distortions in MP π-cation radicals. These authors carried out MNDO/3 semiempirical calculations on zinc porphine (ZnP), which has an a_{1u} HOMO, and on zinc *meso*-tetrafluoroporphine (ZnTFP), which has an a_{2u} HOMO. Extraction of an electron from ZnTFP to give an A_{2u} radical cation increased the $C_{\beta}C_{\beta}$ and $C_{\alpha}C_{m}$ lengths and decreased the $C_{\alpha}C_{\beta}$ lengths, leading to a slight core expansion, whereas extracting an electron from ZnP to give an A_{1u} radical decreased the $C_{\beta}C_{\beta}$ lengths and increased the $C_{\alpha}C_{\beta}$ lengths (consult Figure 1 for the atomic labels). Interestingly, when the symmetry was restricted to D_{4h}, the MNDO/3 calculation failed to converge for ZnP^{+} but not for $ZnTFP^{+}$. Relaxation to D_4 led to a pronounced alternation of the $C_{\alpha}C_{m}$ and $C_{\alpha}N$ bonds of the inner 16-membered ring for ZnP^{+}, but not for $ZnTFP^{+}$. The bond alternation is due to the mixing of the A_{1u} and A_{2u} electronic states along an A_{2g} coordinate. This pJT effect has previously been inferred from the appearance of A_{2g} modes at unusually low frequencies in the RR spectra of MP cation radicals.[19]

Ghosh and co-workers[24] applied for the first time density functional theory (DFT) to investigate the energetics, molecular structures, and spin density profiles of MP π-cation radicals. These studies demonstrated that the common practice to describe these radicals in terms of the A_{1u}/A_{2u} dichotomy is often not justified because the actual picture is further complicated by the pJT effect, as was initially recognized by Spiro and co-workers.[19,23] Ghosh et al.[24] established that the porphyrin π-cation radicals undergo a pJT distortion if the energy difference between the $^2A_{1u}$ and $^2A_{2u}$ π-cation radicals, optimized under D_{4h} symmetry constrains, is less than 0.15 eV. Interestingly, it was concluded that not all MP π-cation radicals are subject to a pJT distortion. For example, employing the energy difference criteria, they showed that metalloporphine (MP) and metallooctaethylporphyrin (MOEP) should always be pJT-distorted, while metallo-*meso*-tetrahalogenoporphyrin radicals should not. When the pJT distortion takes place, a significant bond length alternation around the central 16-membered $C_{12}N_4$ is observed. Because many MPs exist as cofacial dimers in the crystalline phase, Ghosh and co-workers[24] further investigated model compounds $[\{Zn(P)\}_2]^{+,2+}$ employing DFT to obtain the influence of dimer formation on bond lengths in the macrocycles. The results showed that dimerization has relatively little impact on the bond length alternation in the individual rings.

While the aforementioned computational studies have been carried out on divalent complexes, Xu et al.[25] investigated the ground-state geometries and electronic properties of the monolithium porphyrin (LiP) π-radical of related reduced/oxidized species, including $[LiP]^{-}$, $[LiP]^{2-}$, and $[LiP]^{+}$ as well as LiOEP, $[LiOEP]^{-}$, LiTPP, and $[LiTPP]^{-}$, and assessed the effect of the peripheral substitution. It is interesting to note that Li−porphyrins such as LiTPP, LiPFP, or LiTBP are neutral π-radicals, and their EPR spectra show g-values of ∼2.00, consistent with organic free radicals. Employing DFT, Xu et al. showed that LiP, $[LiP]^{-}$, and $[LiP]^{+}$ have planar D_{4h} structure, while the $[LiP]^{2-}$ dianion has a rectangular distorted D_{2h} structure, due to the ground-state Jahn−Teller effect. Furthermore, it was found that the ground state of LiTPP has a normal porphyrin ring with effective D_{4h} symmetry, while the ground-state LiOEP has a porphyrin ring with pronounced bond length alternation and, hence, effective C_{4h} symmetry due to the pJT distortion along an A_{2g}-like coordinate.

The aim of the present work is to investigate, by means of DFT, the structural and electronic properties of MP π-cation radicals, and suggest a resolution of the long-standing problem regarding the nature of the mixed $A_{1u}-A_{2u}$ states of porphyrin radical cations. Emphasis is placed on two issues: the first is associated with structure of the porphyrin ring and the changes associated with the pJT distortion. More specifically, the electronic and structural properties will be placed in the context of the pJT effect and correlated with core size. The second issue addresses the extent of the A_{1u}/A_{2u} mixing by employing orbital projection technique and spin density decomposition.

Results and Discussion

1. Computational Details. All the calculations reported in this work were carried out using nonlocal DFT with the hybrid Becke−Lee−Yang−Parr (B3LYP) functional and the 6-31G-(d) basis set (5d components) as implemented in the Gaussian suite of programs.[26] This level of theory was found to be appropriate for the structural analysis, vibrations, and electronic properties of MPs, leading to excellent agreement with experimental data. To elucidate the structural and electronic properties of π-cation radicals, a series of MPs without peripheral substituents was analyzed, incorporating a variety of transition metals. For each MP under consideration (M = Cr, Mn, Fe, Co, Ni, Cu and Zn), the structure has been fully optimized assuming D_{4h} symmetry, and the resulting electronic configuration was verified to correspond to a stable electronic minimum by performing an analysis of the stability of the wave function. For each optimum geometry, harmonic frequencies were calculated to verify that the optimized structures correspond to stable minima. In all cases, the stable minimum was confirmed, with the exception of Ni−porphine, which possessed one imaginary frequency associated with the ruffling of the porphine macrocycle; this feature was analyzed and explained in previous studies.[28]

Employing these minimized structures as well as optimized wave functions, the series of corresponding π-cation radicals have been generated from neutral MPs by the removal of one electron. The resulting geometries were optimized under D_{4h} symmetry constraints, and the identity of each radical species was verified by natural orbital analysis. In the majority of cases,

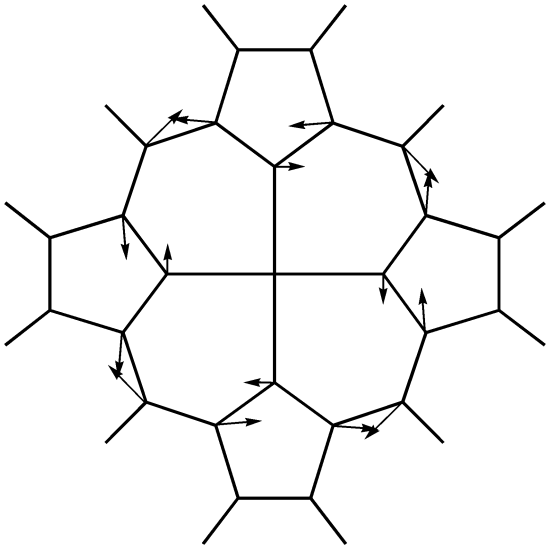

Figure 3. $D_{4h} \rightarrow C_{4h}$ symmetry lowering of a porphine 16-membered ring upon a_{2g} ($a_{1u} \times a_{2u}$) pJT distortion.

the resulting radical was found to be of the A_{1u} type; however, some cases (like MnP) exhibited an A_{2u} type. To generate the second type of radical from an already computed type, the frontier HOMO orbitals were swapped, and the resulting structure was optimized. By imposing symmetry constraints and appropriate orbital occupancy for each MP, a pair of corresponding cation radicals $MP^{\bullet+}(A_{1u})$ and $MP^{\bullet+}(A_{2u})$ was generated for each MP. Frequency analysis showed that none of the $MP^{\bullet+}(A_{1u})$ or $MP^{\bullet+}(A_{2u})$ radicals under the D_{4h} symmetry constraints corresponded to a stable minimum. This finding is consistent with previous theoretical studies and is a consequence of the pJT effect that lowers the symmetry (Figure 3). Consequently, the symmetry of each $MP^{\bullet+}$ radical has been distorted along the imaginary A_{2g} mode, and the structure has been reoptimized with C_{4h} symmetry constraints. At the end of each optimization, the status of the structure with lower symmetry, $MP^{\bullet+}$(mixed), was confirmed to be a stable minimum by frequency analysis.

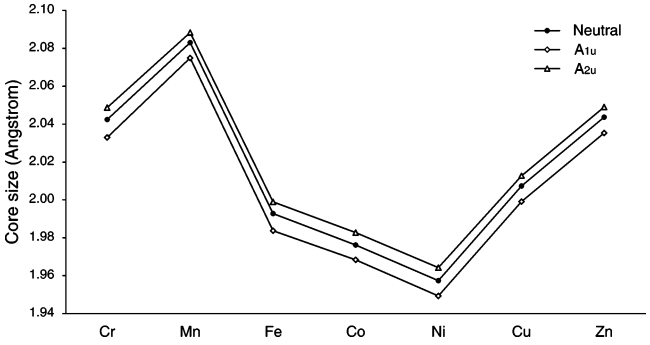

Figure 4. Comparison of core size dependence for MP, $MP^{\bullet+}(A_{1u})$, and $MP^{\bullet+}(A_{2u})$ plotted as a function of metal d^n electrons ($n = 4-10$).

2. Molecular Structure of $MP^{\bullet+}(A_{1u})$ and $MP^{\bullet+}(A_{2u})$ Radicals. The incorporation of transition metals with different occupancies of d-orbitals between 4 and 10 allows one to investigate the MPs with different spin states ranging from singlet to sextet, as well as the coverage of the range of experimentally known metal−nitrogen bond lengths (denoted as $M-N_p$); *the $M-N_p$ bond lengths are commonly referred to as the core size*. The most relevant bond lengths are collected in Table 1. The comparison of the core size dependence for MP, $MP^{\bullet+}(A_{1u})$, and $MP^{\bullet+}(A_{2u})$ plotted as a function of an increasing number of d-electrons is shown in Figure 4. The largest core size (2.083 Å) is observed for MnP, while the shortest core size (1.957 Å) is observed for NiP. The range of computed $M-N_p$ values covers the range of experimentally observed values without complications associated with peripheral substituents. The formation of either an A_{1u}- or an A_{2u}-type radical has a very systematic influence on the core size,

TABLE 1: Symmetry Unique Bond Lengths for MP and Corresponding $MP^{\bullet+}$ Radicals

molecule	M−N	$C_\alpha-N_p$		$C_\alpha-C_{meso}$		$C_\beta-C_\beta$	$C_\alpha-C_\beta$	
CrP	2.0424	1.3768		1.3951		1.3638	1.4440	
$CrP^{\bullet+}(A_{1u})$	2.0330	1.3757		1.3948		1.3528	1.4600	
$CrP^{\bullet+}(A_{2u})$	2.0487	1.3728		1.4027		1.3671	1.4403	
$CrP^{\bullet+}$(mixed)	2.0370	1.3604	1.3898	1.3784	1.4157	1.3563	1.4537	1.4564
MnP	2.0830	1.3722		1.4035		1.3664	1.4481	
$MnP^{\bullet+}(A_{1u})$	2.0749	1.3706		1.4035		1.3554	1.4645	
$MnP^{\bullet+}(A_{2u})$	2.0884	1.3690		1.4108		1.3686	1.4449	
$MnP^{\bullet+}$(mixed)	2.0834	1.3529	1.3867	1.3866	1.4298	1.3635	1.4532	1.4516
FeP	1.9927	1.3793		1.3867		1.3614	1.4398	
$FeP^{\bullet+}(A_{1u})$	1.9837	1.3778		1.3866		1.3505	1.4559	
$FeP^{\bullet+}(A_{2u})$	1.9989	1.3756		1.3939		1.3648	1.4362	
$FeP^{\bullet+}$(mixed)	1.9850	1.3691	1.3862	1.3766	1.3977	1.3515	1.4536	1.4554
CoP	1.9761	1.3806		1.3834		1.3591	1.4399	
$CoP^{\bullet+}(A_{1u})$	1.9684	1.3781		1.3835		1.3485	1.4560	
$CoP^{\bullet+}(A_{2u})$	1.9828	1.3766		1.3907		1.3626	1.4364	
$CoP^{\bullet+}$(mixed)	1.9688	1.3733	1.3828	1.3778	1.3894	1.3488	1.4552	1.4560
NiP	1.9574	1.3808		1.3797		1.3578	1.4385	
$NiP^{\bullet+}(A_{1u})$	1.9493	1.3787		1.3799		1.3474	1.4544	
$NiP^{\bullet+}(A_{2u})$	1.9642	1.3771		1.3870		1.3616	1.4348	
$NiP^{\bullet+}$(mixed)	1.9494	1.3759	1.3812	1.3766	1.3832	1.3475	1.4539	1.4548
CuP	2.0072	1.3756		1.3883		1.3611	1.4429	
$CuP^{\bullet+}(A_{1u})$	1.9990	1.3737		1.3888		1.3506	1.4586	
$CuP^{\bullet+}(A_{2u})$	2.0128	1.3726		1.3957		1.3644	1.4387	
$CuP^{\bullet+}$(mixed)	2.0046	1.3570	1.3902	1.3717	1.4116	1.3556	1.4503	1.4520
ZnP	2.0437	1.3733		1.3957		1.3637	1.4458	
$ZnP^{\bullet+}(A_{1u})$	2.0354	1.3717		1.3958		1.3529	1.4616	
$ZnP^{\bullet+}(A_{2u})$	2.0490	1.3703		1.4030		1.3665	1.4419	
$ZnP^{\bullet+}$(mixed)	2.0412	1.3548	1.3880	1.3781	1.4198	1.3584	1.4525	1.4544

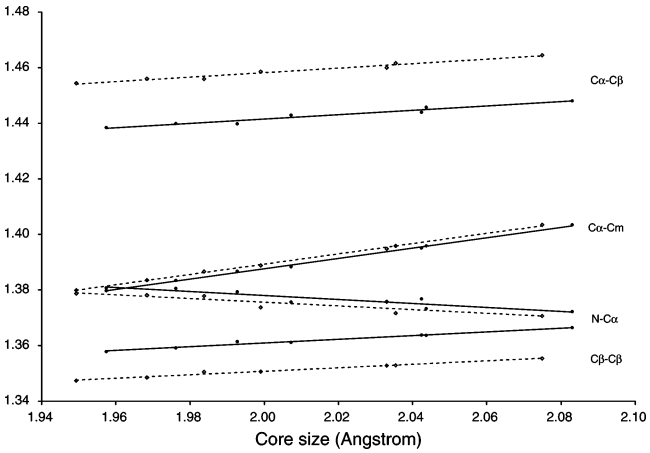

Figure 5. Symmetry unique bond lengths for MP(neutral) and the $MP^{\bullet+}(A_{1u})$ radical plotted as a function of core size. Solid lines represent neutral MPs, while dashed lines represent their π-cation radicals.

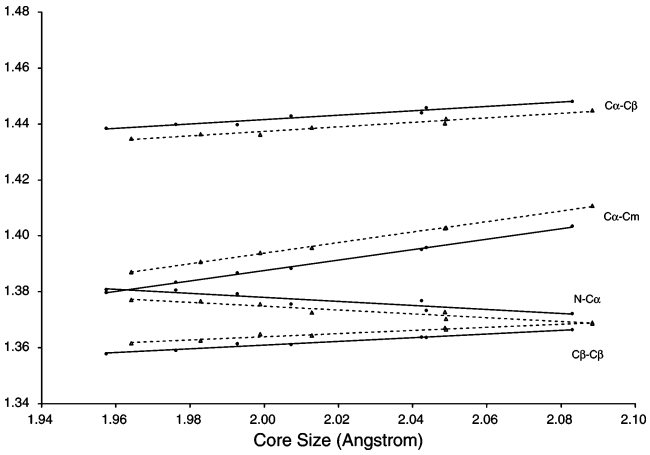

Figure 6. Symmetry unique bond lengths for MP(neutral) and the $MP^{\bullet+}(A_{2u})$ radical plotted as a function of core size. Solid lines represent neutral MPs, while dashed lines represent their π-cation radicals.

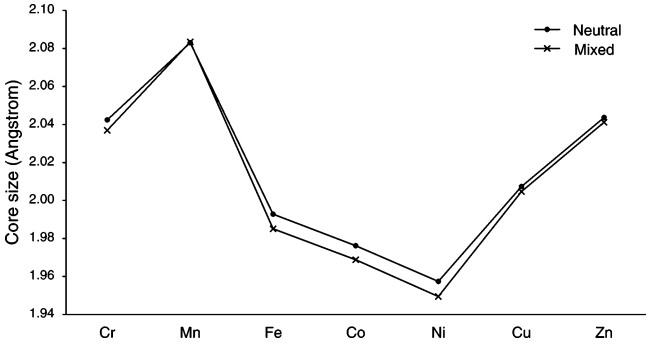

Figure 7. Comparison of core size dependence for MP and $MP^{\bullet+}$-(mixed), plotted as a function of metal d^n electrons ($n = 4-10$).

contrary to the mixed type (see Figure 7). In the A_{1u} radicals, the core size contracts, while, for the A_{2u} type, the core size expands; the degree of contraction or expansion of the core size is very systematic across the range of investigated transition metals (Figure 4).

To further explore geometric changes upon the formation of MP π-cation radicals, the symmetry unique bond lengths were plotted as a function of core size, as shown in Figures 5 and 6. An increase in the bond lengths for $C_\alpha-C_\beta$, $C_\alpha-C_m$, and $C_\beta-C_\beta$ and a decrease for $N-C_\alpha$ is observed for the range of analyzed core sizes (1.96−2.09 Å). With increasing core size, the rigid porphine skeleton compensates by adjusting other

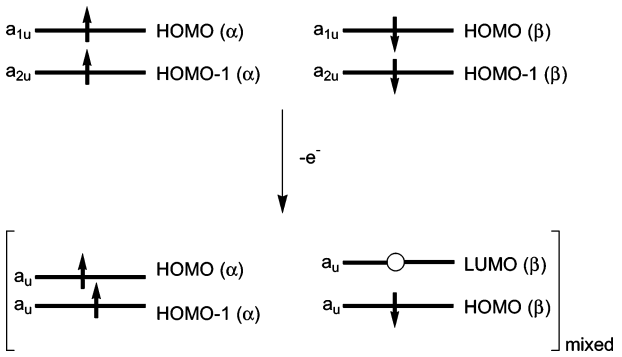

Figure 8. Effects of symmetry lowering and orbital mixing during electron removal.

geometric parameters. Upon removal of an electron from the a_{1u} orbital, the biggest bond lengthening is observed for the $C_\alpha-C_\beta$ bond, due to a loss of π-bonding interaction between C_α and C_β in the a_{1u} orbital. Bond lengthening is also noticeable for $C_\alpha-C_m$ to a lesser degree. On the other hand, the $C_\beta-C_\beta$ bond is shortened because of the alleviation of the antibonding π-type interaction between the two atoms; a slight shortening is also observed for $N-C_\alpha$. These changes are consistent with the nodal pattern of the a_{1u} orbital. When an electron is removed from an a_{2u} orbital, the largest degree of lengthening is observed for $C_\alpha-C_m$, while that for $C_\beta-C_\beta$ is smaller. Shortening is found for both $N-C_\alpha$ and $C_\alpha-C_\beta$, and again these changes are consistent with the nodal pattern of the a_{2u} orbital. These implications of bond length changes are particularly important for understanding the nature of the structure-sensitive vibrations, which can be used as markers of radical formation.

3. pJT Distortions. The structural analysis of the A_{1u} and A_{2u} radicals was performed under the assumption that resulting radicals possess unchanged D_{4h} symmetry of the porphine macrocycle with respect to the neutral MP structure. The actual picture of $MP^{\bullet+}$ is more complicated because the a_{1u} and a_{2u} HOMO orbitals become degenerate, the resulting nuclear and electronic configurations become unstable, and the system experiences a pJT distortion along an a_{2g} ($a_{1u} \times a_{2u}$) coordinate. The consequence of this distortion is a $D_{4h} \rightarrow C_{4h}$ symmetry lowering (Figure 3), upon which $a_{1u}-a_{2u}$ orbital mixing takes place (Figure 8). This particular example of symmetry lowering is demonstrated for the $ZnP^{\bullet+}$(mixed) radical, which shows the extent to which the a_{1u} and a_{2u} orbitals are mixed (Figure 9). The mixed frontier orbitals no longer have a plane of symmetry perpendicular to the plane of the molecule but still possess a center of inversion when symmetries a_{1u} or a_{2u} are effectively lowered to a_u.

The pJT distortion has a pronounced effect on the porphine macrocycle ring, which, upon distortion, results in the structure having alternant bond lengths (Figure 3). The effect of distortion leads to two categories of bonds with respect to the parent neutral MP structure, which can further be denoted as "short" and "long" (see Table 1). When symmetry lowering from D_{4h} to C_{4h} takes place, the bond alternation is primarily observed for the $C_\alpha-C_m$ and $N-C_\alpha$ in the 16-member inner ring. The change in core size (Figure 7) is less systematic than it is in the case of "pure" A_{1u}- or A_{2u}-type radicals (Figure 4). It appears that, for short $M-N_p$ bond lengths (i.e., less than ~2.0 Å), the core size shortens when $MP^{\bullet+}$(mixed) is formed, while the opposite is observed for larger $M-N_p$ bond lengths, where the core size expands for $MP^{\bullet+}$(mixed). These changes in core size may indicate that, for short values, the preference is for the formation of a radical having a dominant A_{1u} character, while,

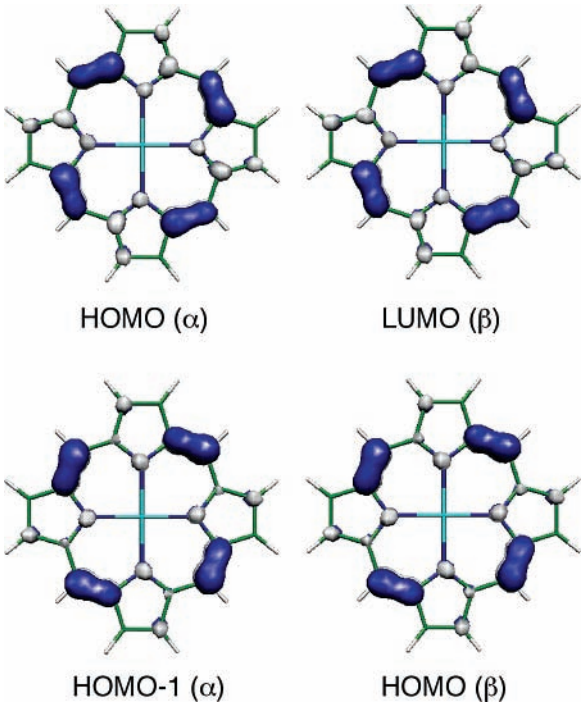

Figure 9. Mixing of the frontier orbitals due to pJT distortion. MOLEKEL software[27] was used to generate molecular orbitals.

for large core size values, the removal of an electron produces a radical that is better characterized as an A_{2u} type.

4. Orbital Decomposition. The analysis of frontier molecular orbitals (MOs) obtained upon pJT mixing (Figure 9) leads to the following two questions: (i) To what extent do the frontier MOs correspond to the ideal a_{1u} and a_{2u} symmetry as shown in Figure 2? and (ii) To what extent does the mixing between them take place? To answer these questions, we applied the orbital decomposition (projection) method, which can be summarized as follows: the Kohn−Sham orbitals (KSOs) of the neutral MP state expressed in terms of the linear combination of atomic orbitals (LCAO) have the form

$$\phi = \chi \mathbf{C} \tag{1}$$

where ϕ and χ are KSOs and basis atomic orbitals (AOs), respectively:

$$\phi = (\phi_1\, \phi_2\, ...\, \phi_N) \tag{2}$$

$$\chi = (\chi_1\, \chi_2\, ...\, \chi_N), \tag{3}$$

and **C** is the matrix of the LCAO−KSO coefficients:

$$\mathbf{C} = \begin{pmatrix} c_{1,1} & c_{1,2} & \cdots & c_{1,N} \\ c_{2,1} & c_{2,2} & \cdots & c_{2,N} \\ \vdots & \vdots & \ddots & \vdots \\ c_{N,1} & c_{N,2} & \cdots & c_{N,N} \end{pmatrix} \tag{4}$$

The *i*th column contains the LCAO−KSO coefficients of the *i*th KSO, and *N* is the number of basis AOs. Similarly, the KSOs of the mixed state are represented as

$$\phi'_\alpha = \chi' \mathbf{C}'_\alpha \tag{5}$$

$$\phi'_\beta = \chi' \mathbf{C}'_\beta \tag{6}$$

Because these two states have very similar structures, here we assume the relation

$$\chi = \chi' \tag{7}$$

Then, the canonical KSOs of the mixed states can be written as

$$\phi'_\alpha = \phi \mathbf{C}^{-1} \mathbf{C}'_\alpha = \phi \mathbf{D}_\alpha \tag{8}$$

$$\phi'_\beta = \phi \mathbf{C}^{-1} \mathbf{C}'_\beta = \phi \mathbf{D}_\beta \tag{9}$$

By analyzing the **D** matrices, the origins of the KSOs of the mixed state can be reliably estimated. That is, the distorted KSOs of the mixed state are now expressed in terms of the KSOs of the neutral state containing pure a_{1u} and a_{2u}; the squared coefficients of these pure orbitals in the mixed ones allow for estimation of the corresponding mixing weights. For the four relevant mixed orbitals (Figure 9), the sum of the squared coefficients for a_{1u} and a_{2u} was almost 1.0 (Table 2), indicating that the mixed orbitals are predominantly composed of a_{1u} and a_{2u}. As such, we further normalized the coefficients by dividing them by $(c_1^2+c_2^2)^{1/2}$, so that the sum of the squared coefficients is exactly 1.0. By this scheme, we can gain insight into the a_{1u}/a_{2u} mixing ratio of the distorted orbitals such as those depicted in Figure 9.

Table 2 provides a summary of frontier orbital decomposition for the four orbitals in Figure 8, in all seven MPs under consideration. For example, the HOMO (α) of the mixed state of ZnP is expressed by the orbitals of the neutral state as $0.810\phi_{a1u} + 0.586\phi_{a2u}$, using the normalized coefficients, and is composed of 65.6% of a_{1u} and 34.4% of a_{2u}.

5. Spin Density Analysis. An alternative analysis of the A_{2u}/A_{1u} composition of $MP^{\bullet+}$ species was carried out by resolving the atomic spin densities into the corresponding contributions from the pure symmetry species. The formation of a MP radical cation is naturally associated with the overall spin change, which, in consequence, leads to the presence of one unpaired electron located on the porphyrin ring. To elucidate the nature of this change, the spin density profiles have been computed for the series of $MP^{\bullet+}$ by means of spin-unrestricted calculations on the corresponding optimized geometries (see Supporting Information for details). The analysis of spin distribution shows that, upon formation of the A_{1u}-type radical, the spin density is primarily located on the C_α and C_β carbons, while, for the A_{2u}-type radical, it is on the N_p and C_{meso} atoms; these spin density distribution patterns are consistent with the atomic contributions to the two highest occupied orbitals (Figure 2).

Unraveling the mixing of electronic states in terms of spin densities is complicated by the presence of unpaired spin density that arises for porphyrins having an open-shell transition metal. To overcome this difficulty, the analysis was shifted toward relative spin densities (Table 3) where the difference in spin densities have been computed as $\Delta\rho = [MP^{\bullet+}(...) - MP]$ with respect to the particular type of radical denoted as $MP^{\bullet+}(...)$. It is interesting to note that the relative spin densities are more systematic and similar to each other, regardless of the specific identity of the $MP^{\bullet+}$. The central metal has small residual value that can be neglected as a first approximation. On average, the biggest change for $MP^{\bullet+}(A_{1u})$ is observed for ΔC_β (0.1773), and the smallest is observed for ΔC_α (0.0241). The overall change in spin density associated with the ΔC_α and ΔC_β pair of atoms multiplied by the total number of α and β carbons in the porphine macrocycle (i.e., eight) gives a value of 1.6112. This is greater than 1, but the difference of 0.6112 is compensated by the negative change in spin density on the ΔN_p

TABLE 2: Projection of Orbitals in the Mixed State into the A_{1u} and a_{2u} Orbitals in the Neutral State

	c_1(raw)[a]	c_2(raw)[a]	c_1(norm)[b]	c_2(norm)[b]	ratio(a_{1u})[c]	ratio(a_{2u})[c]
			CrP			
α-90(HOMO-4)	−0.937	0.336	−0.941	0.337	0.886	0.114
α-94(HOMO)	0.349	0.941	0.348	0.938	0.121	0.879
β-89(HOMO)	0.487	0.867	0.490	0.872	0.240	0.760
β-90(LUMO)	−0.876	0.496	−0.870	0.493	**0.757**	**0.243**
			MnP			
α-93(HOMO-2)	−0.464	0.875	−0.468	0.884	0.219	0.781
α-94(HOMO-1)	0.885	0.480	0.879	0.477	0.773	0.227
β-89(HOMO)	0.791	0.601	0.796	0.605	0.634	0.366
β-90(LUMO)	−0.613	0.799	−0.609	0.793	**0.371**	**0.629**
			FeP			
α-93(HOMO-1)	0.988	0.157	0.988	0.157	0.975	0.025
α-94(HOMO)	−0.165	0.987	−0.165	0.986	0.027	0.973
β-90 (HOMO-1)	0.268	0.960	0.269	0.963	0.072	0.928
β-92(LUMO)	−0.967	0.274	−0.962	0.273	**0.926**	**0.074**
			CoP			
α-93(HOMO-1)	0.996	0.106	0.994	0.105	0.989	0.011
α-94(HOMO)	−0.110	0.994	−0.110	0.994	0.012	0.988
β-92(HOMO)	0.148	0.987	0.149	0.989	0.022	0.978
β-93(LUMO)	−0.993	0.152	−0.989	0.151	**0.977**	**0.023**
			NiP			
α-93(HOMO-1)	−1.000	0.062	−0.998	0.062	0.996	0.004
α-94(HOMO)	0.065	0.997	0.065	0.998	0.004	0.996
β-93(HOMO)	−0.080	0.995	−0.081	0.997	0.006	0.994
β-94(LUMO)	1.001	0.082	0.997	0.082	**0.993**	**0.007**
			CuP			
α-93(HOMO-1)	0.625	0.769	0.631	0.776	0.398	0.602
α-94(HOMO)	−0.780	0.637	−0.774	0.633	0.600	0.400
β-93(HOMO)	0.607	0.786	0.612	0.791	0.374	0.626
β-94(LUMO)	−0.796	0.617	−0.790	0.613	**0.625**	**0.375**
			ZnP			
α-94(HOMO-1)	−0.578	0.806	−0.583	0.813	0.339	0.661
α-95(HOMO)	0.816	0.591	0.810	0.586	0.656	0.344
β-94(HOMO)	−0.654	0.747	−0.659	0.752	0.434	0.566
β-95(LUMO)	0.758	0.664	0.752	0.659	**0.566**	**0.434**

[a] Raw coefficients from the **D** matrix. [b] Normalized coefficients. [c] Calculated from the squared normalized coefficients.

TABLE 3: Spin Density Changes during Electron Ejection from Metalloporphines [$MP^{\bullet+}$(...) − MP]

$MP^{\bullet+}$ radical	ΔM	ΔN_p	ΔC_α		ΔC_{meso}	ΔC_β	
$CrP^{\bullet+}(A_{1u})$	−0.0227	−0.0505	0.0236		−0.0969	0.1779	
$CrP^{\bullet+}(A_{2u})$	0.0064	0.1140	0.0037		0.2999	−0.0801	
$CrP^{\bullet+}$(mixed)	−0.0149	−0.0098	−0.0288	0.0679	−0.0014	0.1557	0.0731
$MnP^{\bullet+}(A_{1u})$	−0.0066	−0.0532	0.0232		−0.1005	0.1795	
$MnP^{\bullet+}(A_{2u})$	0.0061	0.1204	0.0003		0.3039	−0.0816	
$MnP^{\bullet+}$(mixed)	0.0022	0.0585	−0.0387	0.0577	0.1546	0.0567	−0.0311
$FeP^{\bullet+}(A_{1u})$	−0.0093	−0.0505	0.0243		−0.0957	0.1750	
$FeP^{\bullet+}(A_{2u})$	0.0039	0.1096	0.0054		0.2951	−0.0771	
$FeP^{\bullet+}$(mixed)	−0.0080	−0.0383	−0.0066	0.0529	−0.0671	0.1811	0.1309
$CoP^{\bullet+}(A_{1u})$	−0.0244	−0.0540	0.0252		−0.0950	0.1774	
$CoP^{\bullet+}(A_{2u})$	−0.0052	0.1045	0.0061		0.2894	−0.0713	
$CoP^{\bullet+}$(mixed)	−0.0239	−0.0502	0.0411	0.0086	−0.0864	0.1581	0.1852
$NiP^{\bullet+}(A_{1u})$	−0.0162	−0.0540	0.0253		−0.0944	0.1761	
$NiP^{\bullet+}(A_{2u})$	0.0028	0.1025	0.0068		0.2879	−0.0713	
$NiP^{\bullet+}$(mixed)	−0.0160	−0.0529	0.0159	0.0344	−0.0919	0.1819	0.1669
$CuP^{\bullet+}(A_{1u})$	0.0062	−0.0563	0.0242		−0.0976	0.1770	
$CuP^{\bullet+}(A_{2u})$	0.0151	0.1080	0.0030		0.2933	−0.0744	
$CuP^{\bullet+}$(mixed)	0.0104	0.0080	−0.0333	0.0671	0.0489	0.1238	0.0378
$ZnP^{\bullet+}(A_{1u})$	0.0058	−0.0558	0.0235		−0.0998	0.1785	
$ZnP^{\bullet+}(A_{2u})$	0.0147	0.1075	0.0030		0.2971	−0.0760	
$ZnP^{\bullet+}$(mixed)	0.0106	0.0129	−0.0358	0.0675	0.0610	0.1184	0.0284
$MP^{\bullet+}(A_{1u})_{average}$		**−0.0535**	**0.0241**		**−0.0971**	**0.1773**	
$MP^{\bullet+}(A_{2u})_{average}$		**0.1095**	**0.0040**		**0.2952**	**−0.0760**	

and ΔC_{meso} atoms, which is equal to −0.6024. In the case of the $MP^{\bullet+}(A_{2u})$ radical, the biggest change is observed for ΔC_{meso}, which is equal to 0.2952, and that for ΔN_p is almost 3 times smaller, being 0.1095. Again, the total balance of spin density gives a value of 1.6188 for all four ΔN_p and ΔC_{meso} atoms, which is essentially compensated by the negative change in ΔC_β with an overall value of 0.608.

The spin change associated with the radicals described as $MP^{\bullet+}$(mixed) is not systematic. To explore the extent of mixing in terms of A_{1u} and A_{2u} components, it was found that the use

TABLE 4: Group Spin Density $\Delta\rho(N,C_m)^a$ and $\Delta\rho(C_\alpha,C_\beta,C_\alpha',C_\beta')^b$ Based on Relative Spin Density Values [$MP^{\bullet+}$(...) − MP]

	ΔN_p	ΔC_{meso}	$\Delta\rho(N,C_m)$	ΔC_α		ΔC_β		$\Delta\rho(C_\alpha,C_\beta,C_\alpha',C_\beta')$
$CrP^{\bullet+}(A_{1u})$	−0.0505	−0.0969	−0.1474	0.0236		0.1779		0.4029
$CrP^{\bullet+}(A_{2u})$	0.1140	0.2999	0.4139	0.0037		−0.0801		−0.1528
$CrP^{\bullet+}$(mixed)	−0.0098	−0.0014	**−0.0112**	−0.0288	0.0679	0.1557	0.0731	**0.2679**
$MnP^{\bullet+}(A_{1u})$	−0.0532	−0.1005	−0.1537	0.0232		0.1795		0.4054
$MnP^{\bullet+}(A_{2u})$	0.1204	0.3039	0.4243	0.0003		−0.0816		−0.1628
$MnP^{\bullet+}$(mixed)	0.0585	0.1546	**0.2131**	−0.0387	0.0577	0.0567	−0.0311	**0.0446**
$FeP^{\bullet+}(A_{1u})$	−0.0505	−0.0957	−0.1462	0.0243		0.1750		0.3986
$FeP^{\bullet+}(A_{2u})$	0.1096	0.2951	0.4047	0.0054		−0.0771		−0.1434
$FeP^{\bullet+}$(mixed)	−0.0383	−0.0671	**−0.1054**	−0.0066	0.0529	0.1811	0.1309	**0.3583**
$CoP^{\bullet+}(A_{1u})$	−0.0540	−0.0950	−0.1490	0.0252		0.1774		0.4053
$CoP^{\bullet+}(A_{2u})$	0.1045	0.2894	0.3939	0.0061		−0.0713		−0.1304
$CoP^{\bullet+}$(mixed)	−0.0502	−0.0864	**−0.1366**	0.0411	0.0086	0.1581	0.1852	**0.3930**
$NiP^{\bullet+}(A_{1u})$	−0.0540	−0.0944	−0.1484	0.0253		0.1761		0.4027
$NiP^{\bullet+}(A_{2u})$	0.1025	0.2879	0.3904	0.0068		−0.0713		−0.1290
$NiP^{\bullet+}$(mixed)	−0.0529	−0.0919	**−0.1448**	0.0159	0.0344	0.1819	0.1669	**0.3991**
$CuP^{\bullet+}(A_{1u})$	−0.0563	−0.0976	−0.1539	0.0242		0.1770		0.4025
$CuP^{\bullet+}(A_{2u})$	0.1080	0.2933	0.4014	0.0030		−0.0744		−0.1428
$CuP^{\bullet+}$(mixed)	0.0080	0.0489	**0.0569**	−0.0333	0.0671	0.1238	0.0378	**0.1933**
$ZnP^{\bullet+}(A_{1u})$	−0.0558	−0.0998	−0.1556	0.0235		0.1785		0.4040
$ZnP^{\bullet+}(A_{2u})$	0.1075	0.2971	0.4046	0.0030		−0.0760		−0.1459
$ZnP^{\bullet+}$(mixed)	0.0129	0.0610	**0.0739**	−0.0358	0.0675	0.1184	0.0284	**0.1784**
$MP^{\bullet+}(A_{1u})_{average}$			**−0.1506**					**0.4028**
$MP^{\bullet+}(A_{2u})_{average}$			**0.4047**					**−0.1440**

^{a} $\Delta\rho(N,C_m) = \Delta(N) + \Delta(C_{meso})$. ^{b} $\Delta\rho(C_\alpha,C_\beta,C_\alpha',C_\beta') = \Delta(C_\alpha) + \Delta(C_\beta) + \Delta(C_\alpha') + \Delta(C_\beta')$.

of group of atoms is more effective toward this end than the use of the spin density changes of individual atoms. Consequently, two groups of atoms have been introduced. The first group is a sum of the α and β carbons, and the overall change of spin density associated them consequently is defined as

$$\Delta\rho(C_\alpha,C_\beta,C_\alpha',C_\beta') = \Delta C_\alpha + \Delta C_\beta + \Delta C_\beta' + \Delta C_\alpha' \quad (10)$$

where the prime label distinguishes nonequivalent carbon atoms in the pyrrole ring upon the pJT distortion. The second group is defined as a pair of nitrogen and meso carbon atoms; the net spin change associated with them is as follows:

$$\Delta\rho(N_p,C_{meso}) = \Delta N_p + \Delta C_{meso} \quad (11)$$

These two groups of definitions are in fact consequences of an orbital pattern observed for the two highest MOs of symmetry, a_{1u} and a_{2u}, respectively. The a_{1u} orbital is mainly concentrated on C_α and C_β, while the a_{2u} is concentrated on N_p and C_{meso} (Figure 2). Following this through, the change of spin profiles can now be described in terms of two quantities, that is, $\Delta\rho(C_\alpha,C_\beta,C_\alpha',C_\beta')$ and $\Delta\rho(N_p,C_{meso})$, as summarized in Table 4. Again, the point of interest is the average spin density change for both groups, which, in the case of the A_{1u} radical is 0.4028 and −0.1506, while, for the A_{2u} type, it is −0.1440 and 0.4047, respectively. The sum in both cases gives nearly 0.25 as one should expect for a quarter of the molecule. Using the definitions of the group spin densities given by eqs 10 and 11, the change of overall spin density upon the formation of A_{1u}-type or A_{2u}-type radicals can be expressed in terms of two component quantities defined as

$$\Delta\rho_{A1u} = [\Delta\rho_{A1u}(C_\alpha,C_\beta,C_\alpha',C_\beta'), \Delta\rho_{A1u}(N,C_{meso})] \quad (12)$$

and

$$\Delta\rho_{A2u} = [\Delta\rho_{A2u}(C_\alpha,C_\beta,C_\alpha',C_\beta'), \Delta\rho_{A2u}(N,C_{meso})] \quad (13)$$

Similarly, the change in spin density in the case of the mixed state is expressed as follows:

$$\Delta\rho_{mix} = [\Delta\rho_{mix}(C_\alpha,C_\beta,C_\alpha',C_\beta'), \Delta\rho_{mix}(N,C_{meso})] \quad (14)$$

On the basis of the above, it is therefore reasonable to express the $\Delta\rho_{mix}$ quantity as a linear combination of $\Delta\rho_{A1u}$ and $\Delta\rho_{A2u}$ components:

$$\Delta\rho_{mix} = c_1\Delta\rho_{A1u} + c_2\Delta\rho_{A2u} \quad (15)$$

The resultant c_1 and c_2 coefficients, obtained by solving simultaneous equations, were normalized by dividing each of the coefficients by $c_1 + c_2$.

It should be noted that the above protocol does not allow for the mixing of $\Delta\rho(C_\alpha,C_\beta,C_\alpha',C_\beta')$ and $\Delta\rho(N,C_{meso})$ components. This approach will further be referred to as decomposition method 1 (DM1). The alternative approach, allowing for the mixing of both components, will be referred to as decomposition method 2 (DM2). In this case, eq 15 simply becomes eq 16:

$$\Delta\rho_{mix} = c_1\Delta\rho_{a1u} + c_2\Delta\rho_{a2u} \quad (16)$$

with similar constraints (i.e., $c_1 + c_2 = 1$) imposed for linear coefficients. Here, $\Delta\rho_{a1u}$ is the sum of the spin density differences at $C_\alpha,C_\beta,C_\alpha',C_\beta'$, N, and C_{meso}, and thus we do not separate the regions as in DM1. These two equations allow us to obtain c_1 and c_2 values.

Both the DM1 and DM2 protocols have been numerically tested and applied to the decomposition of the mixed spin density with respect to A_{1u} and A_{2u} components. The optimal sets of c_1 and c_2 coefficients by DM1 for all seven MP(mixed) radicals are summarized in Table 5. Both DM1 and DM2 protocols predict essentially the same extent of mixing between A_{1u} and A_{2u}, with the exception of the $ZnP^{\bullet+}$(mixed) radical, which shows sensitivity with respect to the applied protocol. However, its dependence can be explained by the fact that, in the case of $ZnP^{\bullet+}$, the mixing of A_{1u} and A_{2u} is almost equal and thus allows the components of spin groups to be used for additional mixing, thus having a noticeable influence on the final results. In other cases, when one type of radical has a dominant contribution, both methods give essentially the same results.

6. Comparison of Orbital Decomposition Results and Spin Density Analysis. The most interesting observation is the close similarities for optimization of the coefficients determined by

TABLE 5: Group Spin Density $\Delta\rho(N,C_m)$[a] and $\Delta\rho(C_\alpha,C_\beta,C_\alpha',C_\beta')$[b] Based on Relative Spin Density Values [$MP^{\bullet+}$(...) − MP]

$MP^{\bullet+}$ radical	$\Delta\rho(N,C_m)$	$\Delta\rho(C_\alpha,C_\beta,C_\alpha',C_\beta')$	c_1 [c]	c_2 [c]	c_1 [d]	c_2 [d]
$CrP^{\bullet+}(A_{1u})$	−0.1474	0.4029				
$CrP^{\bullet+}(A_{2u})$	0.4139	−0.1528				
$CrP^{\bullet+}$(mixed)	−0.0112	0.2679	0.757	0.243	0.783	0.217
$MnP^{\bullet+}(A_{1u})$	−0.1537	0.4054				
$MnP^{\bullet+}(A_{2u})$	0.4243	−0.1628				
$MnP^{\bullet+}$(mixed)	0.2131	0.0446	0.365	0.635	0.384	0.616
$FeP^{\bullet+}(A_{1u})$	−0.1462	0.3986				
$FeP^{\bullet+}(A_{2u})$	0.4047	−0.1434				
$FeP^{\bullet+}$(mixed)	−0.1054	0.3583	0.926	0.074	0.935	0.064
$CoP^{\bullet+}(A_{1u})$	−0.1490	0.4053				
$CoP^{\bullet+}(A_{2u})$	0.3939	−0.1304				
$CoP^{\bullet+}$(mixed)	−0.1366	0.3930	0.977	0.023	0.980	0.020
$NiP^{\bullet+}(A_{1u})$	−0.1484	0.4027				
$NiP^{\bullet+}(A_{2u})$	0.3904	−0.1290				
$NiP^{\bullet+}$(mixed)	−0.1448	0.3991	0.993	0.007	0.994	0.006
$CuP^{\bullet+}(A_{1u})$	−0.1539	0.4025				
$CuP^{\bullet+}(A_{2u})$	0.4014	−0.1428				
$CuP^{\bullet+}$(mixed)	0.0569	0.1933	0.620	0.380	0.644	0.356
$ZnP^{\bullet+}(A_{1u})$	−0.1556	0.4040				
$ZnP^{\bullet+}(A_{2u})$	0.4046	−0.1459				
$ZnP^{\bullet+}$(mixed)	0.0739	0.1784	0.590	0.410	0.618	0.382

[a] $\Delta\rho(N,C_m) = \Delta(N) + \Delta(C_{meso})$. [b] $\Delta\rho(C_\alpha,C_\beta,C_\alpha',C_\beta') = \Delta(C_\alpha) + \Delta(C_\beta) + \Delta(C_\alpha') + \Delta(C_\beta')$. [c] DM1. [d] DM2.

employing the orbital projection technique applied to the β-lowest unoccupied molecular orbital (β-LUMO) and spin density technique based on the DM1 protocol. This is consistent with Figure 8, which shows that the origin of net spin density difference used for the spin density analysis actually corresponds to the hole from which the electron was removed. The hole has a character of the mixed β-LUMO, and is comprised of a mixture of the a_{1u} and a_{2u} orbitals. Consequently, the a_{1u}/a_{2u} ratio of the β-LUMO should reflect the A_{1u}/A_{2u} ratio, since these orbitals characterize this state. In the orbital analysis (eqs 8 and 9), the mixed orbitals were expressed in terms of the pure a_{1u} and a_{2u} components. This is similar to the condition imposed in the DM1 protocol (eqs 12−16), in which the spin density associated with the groups $\{C_\alpha,C_\beta'C_\alpha'C_\beta'\}$ and $\{N_p,C_{meso}\}$ were not allowed to mix. Therefore, the orbital projection and the DM1 scheme both have constrained character and show essentially the same trends, despite the difference in the applied procedure.

When the two electronic states mix, the spin density distribution may get delocalized over the whole molecule. The DM2 protocol was applied in order to take into account such a situation. Consequently, in the DM2 scheme, constrains were not imposed on the spin densities, and flexibility with respect to mixing was fully allowed. When one electronic state has a dominant character, as, for example, in the case of NiP, both DM1 and DM2 protocols give essentially the same results. In cases where both states have similar contributions, as for ZnP, the predictions based on DM1 and DM2 are different, and the estimate provided by the DM2 protocol seems to be more reliable.

The problems of electronic states mixing in terms of spin density decomposition and orbital decomposition are, in fact, related in a qualitative manner. Thus, let us assume that we can write the wave function of the radical cation, MP^+, with $2n-1$ electrons in terms of a closed shell part in $n-1$ closed-shell orbitals, $(\psi_{1(\alpha)}\psi_{1(\beta)}\psi_{2(\alpha)}\psi_{2(\beta)}\cdots\psi_{n-1(\alpha)}\psi_{n-1(\beta)})$ and a single electron in the orbital, $\psi_{n(\alpha)}$, from which one electron was ejected:

$$\Psi_{MP^+} = |(\psi_{1(\alpha)}\psi_{1(\beta)}\psi_{2(\alpha)}\psi_{2(\beta)}\cdots\psi_{n-1(\alpha)}\psi_{n-1(\beta)})\,\psi_{n(\alpha)}| \quad (17)$$

The doubly occupied orbital shell may be associated, for example, with a simple spin-restricted wave function or with a set of corresponding orbitals made from an open-shell wave function, or even with natural orbitals with occupancies close to 2.0. The nature of the orbitals in the closed-shell part is not so important, since the closed-shell part of the Slater determinant in eq 17 is invariant to orbital transformation (unitary transformation). Therefore, we may consider these orbitals to be identical for the neutral MP and its radical cation. As such, if the singly occupied orbital has a mixed character, $\psi_{n(\alpha)}$, and is a linear combination of the corresponding pure symmetry a_{1u} and a_{2u} orbitals,

$$\psi_{n(\alpha)} = a_1\psi_{a1u(\alpha)} + a_2\psi_{a2u(\alpha)} \quad (18)$$

The total wave function of the radical cation would then be expressed as a linear combination of A_{1u} and A_{2u} components:

$$\Psi_{MP^+} = a_1|(\psi_{1(\alpha)}\psi_{1(\beta)}\psi_{2(\alpha)}\psi_{2(\beta)}\cdots\psi_{n-1(\alpha)}\psi_{n-1(\beta)})\psi_{a1u(\alpha)}| + a_2|(\psi_{1(\alpha)}\psi_{1(\beta)}\psi_{2(\alpha)}\psi_{2(\beta)}\cdots\psi_{n-1(\alpha)}\psi_{n-1(\beta)})\,\psi_{a2u(\alpha)}| \quad (19)$$

which are weighted by the corresponding orbital coefficient of the orbital from which the electron was ejected, which is also the LUMO of the radical cation. Of course, the weights of the A_{1u} and A_{2u} components will be given by the square of these coefficients. While this is a qualitative explanation, it nevertheless serves to link the two methods of state projection.

Conclusions

We have presented here a pJT analysis of radical cations of $MP^{\bullet+}$ species and developed three methods for projecting the amounts of pure A_{2u} and A_{1u} components in the resulting states. One method is based on projection of the mixed orbitals into their a_{2u} and a_{1u} components, and the other two (DM1 and DM2) are based on an expansion of the changes in the group spin densities into weighted changes of the A_{2u} and A_{1u} components. When one compares the projected A_{2u} and A_{1u} weights of the LUMO to those of the spin-density-based DM1 method, the results are in very good agreement. A qualitatively simple rationale shows why the two methods are actually linked. Of course, one caveat with the orbital projection method is the assumption that the AOs of the MP and $MP^{\bullet+}$ species are identical. This is, of course, not true in the general case of strong distortion (such as ruffling or doming). However, our preliminary results show that, even in such cases, the results of the orbital projection and DM1 techniques are very similar. As such, these methods will be applied in the future to the analyses of more complex MPs with ring substituents and to species of heme enzymes.

Acknowledgment. The research of S.S. and H.H. was supported by a DIP grant from BMBF-DIP (Grant No. DIP-G.7.1). The sabbatical stay of P.M.K. at the HU was supported by The Fulbright Foundation, and in part by the Lise Meitner-Minerva Center for Computational Quantum Chemistry.

Supporting Information Available: Complete citation of reference 26 and a table of the atomic spin population densities. This material is available free of charge via the Internet at http://pubs.acs.org.

References and Notes

(1) Dolphin, D., Ed. *The Porphyrins*; Academic Press: New York, 1978; Vols. I−VI.

(2) Kadish, K. M.; Smith, K. M.; Guilard R., Eds. *The Porphyrin Handbook*; Academic Press: San Diego, CA, 2000.

(3) Dunford, H. B. *Heme Peroxidases*; Wiley−VCH: New York, 1999.

(4) Ortiz de Montellano, P. R., Ed. *Cytochrome P450: Structure, Mechanisms and Biochemistry*, 2nd ed.; Plenum Press: New York, 1995.

(5) Chelikani, P.; Fieta, I.; Loewen, P. C. *Cell. Mol. Life Sci*. **2004**, *61*, 192−208.

(6) Dolphin, D.; Felton, R. H. *Acc. Chem. Res.* **1974**, *7*, 26−32.

(7) Browett, W. R.; Stillman, M. J. *Inorg. Chim. Acta* **1981**, *49*, 69−77. (b) Browett, W. R.; Stillman, M. J. *Biochim. Biophys. Acta* **1981**, *660*, 1−7.

(8) Groves, J. T.; Haushalter, R. C.; Nakamura, M.; Nemo, T. E.; Evans, B. J. *J. Am. Chem. Soc.* **1981**, *103*, 2884−2886.

(9) Phillippi, M. A.; Goff, H. M. *J. Am. Chem. Soc.* **1982**, *104*, 6026−6034.

(10) Morishima, I.; Shiro, Y.; Takamuki, Y. *J. Am. Chem. Soc*. **1983**, *105*, 6168−6170. (b) Morishima, I.; Takamuki, Y.; Shiro, Y. *J. Am. Chem. Soc.* **1984**, *106*, 7666−7672.

(11) Nakashima, S.; Ohya-Nishiguchi, H.; Hirota, N.; Fujii, H.; Morishima, I. *Inorg. Chem.* **1990**, *29*, 5207−5211.

(12) Fujii, H.; Ichikawa, K. *Inorg. Chem.* **1992**, *31*, 1110−1112. (b) Fujii, H. *J. Am. Chem. Soc.* **1993**, *115*, 4641−4648. (c) Fujii, H. *Inorg. Chem.* **1993**, *32*, 875−879. (d) Fujii, H. *Chem. Lett.* **1994**, 1491.

(13) Kitagawa, T.; Mizutani, Y. *Coord. Chem. Rev.* **1994**, *135/136*, 685−735.

(14) Czarnecki, K.; Proniewicz, L. M.; Fujii, H.; Kincaid, J. R. *J. Am. Chem. Soc.* **1996**, *118*, 4680−4685.

(15) Fujii, H.; Yoshimura, T.; Kamada, H. *Inorg. Chem.* **1996**, *35*, 2373−2377. (b) Fujii, H.; Yoshimura, T.; Kamada, H. *Inorg. Chem.* **1997**, *36*, 6142−6143.

(16) Terner, J.; Gold, A.; Weiss, R.; Mandon, D.; Trautwein, A. X. *J. Porphyrins Phthalocyanines* **2001**, *5*, 357−364.

(17) Fujii, H. *Coord. Chem. Rev.* **2002**, *226*, 51−60.

(18) Oertling, W. A.; Salehi, A.; Chung, Y. C.; Leori, G. E.; Chang, C. K.; Babcock G. T. *J. Phys. Chem.* **1987**, *91*, 5887−5898.

(19) Czenuszewicz, R. S.; Macor, K. A.; Li, X.-Y.; Kincaid, J. R.; Spiro, T. G. *J. Am. Chem. Soc*. **1989**, *111*, 3860−3869.

(20) Fajer, J.; Davis, M. S. In *The Porphyrins*; Dolphin, D., Ed.; Academic Press: New York, 1978; Vol. III, Part A, Chapter 4, pp 197−256.

(21) Song, H.; Reed, C. A.; Scheidt, W. R. *J. Am. Chem. Soc*. **1989**, *111*, 6867.

(22) Song, H.; Orosz, R. D.; Reed, C. A.; Scheidt, W. R. *Inorg. Chem.* **1990**, *29*, 4274.

(23) Prendergast, K.; Spiro, T. G. *J. Phys. Chem.* **1991**, *95*, 9728−9736.

(24) Vangberg, T.; Lie, R.; Ghosh, A. *J. Am. Chem. Soc*. **2002**, *124*, 8122−8130.

(25) Xu, L.-C.; Li, Z.-Y.; He T.-J.; Liu, F.-C.; Chen D.-M. *Chem. Phys.* **2004**, *305*, 165−174.

(26) Frisch, M. J. et al. *Gaussian 03*, revision C.02; Gaussian, Inc.: Wallingford, CT, 2004.

(27) Flükiger, P.; Lüthi, H. P.; Portmann, S.; Weber, J. *MOLEKEL 4.2*; Swiss Center for Scientific Computing: Manno, Switzerland, 2000−2002. (b) Portmann, S.; Lüthi, H. P. *Chimia* **2000**, *54*, 766−770.

(28) Kozlowski, P. M.; Rush, T. S., III; Jarzecki, A. A.; Zgierski, M. Z.; Chase, B.; Piffat, C.; Ye, B.-H.; Li, X.-Y.; Pulay, P.; Spiro, T. G. *J. Phys. Chem. A* **1999**, *103*, 1357−1366.